JOURNAL OF COMPUTATIONAL PHYSICS **140,** 400–420 (1998)
ARTICLE NO. CP975888

Two-Level Hierarchical FEM Method for Modeling Passive Microwave Devices

Sergey V. Polstyanko*,[1] and Jin-Fa Lee†

*Ansoft Corporation, 4 Station Square, Suite 660, Pittsburgh, Pennsylvania, 15219;
† ECE Department, WPI, 100 Institute Rd., Worcester, Massachusetts 01609
E-mail: sergey@ansoft.com, jinlee@ee.wpi.edu

Received March 3, 1997; revised November 13, 1997

In recent years multigrid methods have been proven to be very efficient for solving large systems of linear equations resulting from the discretization of positive definite differential equations by either the finite difference method or the h-version of the finite element method. In this paper an iterative method of the multiple level type is proposed for solving systems of algebraic equations which arise from the p-version of the finite element analysis applied to indefinite problems. A two-level V-cycle algorithm has been implemented and studied with a Gauss–Seidel iterative scheme used as a smoother. The convergence of the method has been investigated, and numerical results for a number of numerical examples are presented.

Key Words: approximations and expansions; finite elements; Rayleigh–Ritz and Galerkin methods; finite methods.

1. INTRODUCTION

Modern engineering design relies heavily on numerical simulations. In particular, in electromagnetics, it is often necessary to solve partial differential equations (PDE) on complicated geometries. To solve such PDE numerically, two common discretization methods are used: the finite difference method (FDM) and the finite element method (FEM). Both methods start with a discretization of a given geometry. Such discretization may involve hundreds of thousands of unknowns, and efficient numerical methods are needed to solve a system of linear equations. For matrix equations with very large dimensions, direct methods (based on Gaussian elimination and its variants) require too much memory and prohibitive computational time. Therefore, iterative matrix solutions are necessary for these large problems. However, the rates of convergence of various methods are sensitive to the nature of the problem solved. For this reason no one method may be claimed to be the best for all

[1] SVP was affiliated with ECE Dept., WPI, Worcester, MA 01609.

0021-9991/98 $25.00

problems. Along with the development of new iterative methods, the problem of accelerating the convergence of known iterative methods is of considerable interest from a practical point of view. Developments in both directions have taken place in recent years.

In this paper we shall discuss multigrid methods that have been developed for accelerating the convergence of iterative methods [1, 2]. Multigrid methods [3–10] offer an alternative to efficiently solving large problems, while incurring low additional memory overheads. A notable property of a well-formulated multigrid algorithm is that the number of multigrid cycles required to achieve a given level of convergence is independent of the mesh size h. Thus, multigrid methods enable solutions to be obtained in $O(N)$ operations, where N is the degree of freedom. Linear complexity of this type is considered to be optimal.

The basic idea behind the multigrid algorithm is to work not with a single grid, but with a sequence of grids ("levels") of increasing fineness, each of which may be introduced and changed in the process and constantly interacts with each other [6]. The method iteratively solves a system of discrete (finite-difference or finite-element) equations on a given grid by constant interactions with a hierarchy of coarser grids, taking advantage of the relations between different discretizations of the same continuous problem. The motivation for this approach comes from an examination of the error of the numerical solution in the frequency domain. High frequency errors, which involve local variations in the solution, are well eliminated by simple iterative smoothing methods (iterative matrix solution techniques such as the preconditioned conjugate gradient (PCCG) method, Jacobian iterations). Furthermore, coarse grids can be viewed as correction grids, accelerating convergence of a relaxation scheme on the finest grid by efficiently liquidating smooth error components.

Typically, a multigrid scheme begins by eliminating the high frequency errors associated with an initial solution on the fine grid, using an iterative matrix solver. Once this is achieved, further fine-grid iterations would result only in a convergence degradation. Therefore, the solution is transferred to a coarser grid by using a specified projection operator. On this grid, the low frequency errors of the fine grid manifest themselves as high frequency errors and are thus eliminated efficiently using the same iterative matrix solver (or direct solver on the coarsest grid). The coarse-grid corrections computed on the coarser grid are then interpolated back to the fine grid in order to update the solution. This procedure can be applied recursively on a sequence of coarser and coarser grids, where each grid level is responsible for eliminating a particular frequency bandwidth of errors.

In this work we have made an attempt to combine the multigrid concept with the p-version of the transfinite element approach that has been implemented for the analysis of unbounded problems such as MMIC devices and 3D waveguide junctions [11, 12]. To achieve this goal we have developed a multi-p V-cycle algorithm and studied its performance on sample problems. This paper is organized as follows: in Section 2 we discuss transfinite element method for the analysis of multiport structures, in Section 3 a multi-p algorithm for the p-version of the finite element method is introduced, and in Section 4 we present numerical studies of the multi-p V-cycle. Finally, concluding remarks are given in Section 5.

2. TRANSFINITE ELEMENT FORMULATION FOR MULTIPLE PORTS

To be able to analyze real life passive microwave devices, three-dimensional analysis is required for modeling MMIC devices and waveguide junctions. In this section we shall describe the transfinite element method (TFEM) for the analysis of multiport waveguide

junctions [11, 12]. The basis of this approach is to combine tangential vector finite element basis functions with modal basis functions to provide solutions for open boundary problems. Furthermore, since field solutions for the two-dimensional port regions are unknown, we use a two-dimensional finite element program to solve for the unknown modal field distributions [13].

2.1. *The Boundary Value Problem*

A simple example of a multiport waveguide junction is shown in Fig. 1. It consists of a discontinuity region (Ω_0) of an arbitrary shape coupled at ports by two-dimensional waveguide regions (Ω_i) with arbitrary cross subsections. The field in the discontinuity region (Ω_0) and in the port regions (Ω_i) extending to infinity satisfies the following Helmholtz equation, together with boundary conditions

$$\begin{aligned} \nabla \times \frac{1}{\mu_r} \nabla \times \mathbf{E} - k_0^2 \epsilon_r \mathbf{E} = 0 \quad & (\Omega_0) \\ \mathbf{E}^i = \mathbf{E}^i_{\text{inc}} + \sum_{j=1}^{N} a_j^i \mathbf{E}_j^i \quad & (\Omega_i) \\ \mathbf{n} \times \mathbf{E} = 0 \quad & \text{on } \Gamma, \end{aligned} \tag{1}$$

where $k_0^2 = \omega^2 \mu_0 \epsilon_0$, $\mathbf{E}_j^i$ is the jth mode of the waveguide i, $\mathbf{E}^i_{\text{inc}}$ is the excitation mode for the waveguide i, and a_j^i is the modal coefficient to be solved. Furthermore, we set the number of ports to be M and for each port we specify the first N modes. Since in Eqs. (1) the amplitude of the modal electric field $\mathbf{E}_j^i$ is arbitrary we normalize $\mathbf{E}_j^i$ to give the unity pointing vector

$$\oint_{\Gamma_i} \mathbf{E}_k^i \times \mathbf{H}_k^i \cdot d\mathbf{A} = K_{kk}^i = \begin{cases} 1 & \text{for propagating mode,} \\ j & \text{for evanescent mode,} \end{cases} \tag{2}$$

where $\mathbf{H}_j^i$ is the magnetic field of the jth mode of the waveguide i and $j = \sqrt{-1}$.

2.2. *The Bilinear Form*

In order to solve Eqs. (1), Galerkin's weighted residual approach has been used to construct our finite element formulation and leads to a symmetric matrix given later. Application of Galerkin's method to the current BVP results in the bilinear form

$$B(\boldsymbol{\mathcal{E}}, \boldsymbol{\mathcal{V}}) = \int_{\Omega_0} (\nabla \times \boldsymbol{\mathcal{V}}) \cdot \frac{1}{\mu_r} (\nabla \times \boldsymbol{\mathcal{E}}) - k_0^2 \boldsymbol{\mathcal{V}} \cdot \epsilon_r \boldsymbol{\mathcal{E}} \, d\Omega - \sum_{m=1}^{M} \oint_{\Gamma_m} \boldsymbol{\mathcal{V}} \times \frac{1}{\mu_r} (\nabla \times \boldsymbol{\mathcal{E}}) \cdot d\mathbf{A}, \tag{3}$$

where $\boldsymbol{\mathcal{V}}, \boldsymbol{\mathcal{E}}$ are the testing and trial fields, respectively. To form the bilinear form (3), we have employed Green's theorem and set the testing and trial spaces to be the same and denoted it by Λ. In the Galerkin's process, we need to find a solution vector function $\boldsymbol{\mathcal{E}}$ such that $B(\boldsymbol{\mathcal{E}}, \boldsymbol{\mathcal{V}}) = 0$ for every vector function $\boldsymbol{\mathcal{V}}$ in the infinite-dimensional space Λ. Furthermore, in the finite element process we replace Λ by a finite-dimensional space Λ^h contained in Λ.

The transfinite element method begins by selecting a suitable subspace Λ^h. Notice that in Fig. 1 we have separated the problem domain into two parts: the discontinuity region

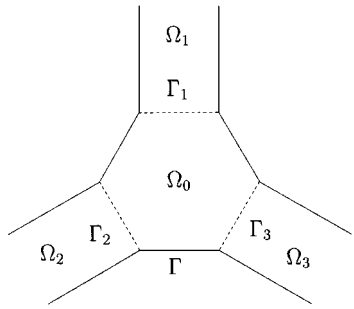

FIG. 1. Multiport waveguide junction.

(Ω_0) and the waveguide regions (Ω_i). In the TFEM formulation we use finite element basis functions for modeling the inhomogeneities and irregular geometries in the finite-sized discontinuity region (Ω_0) and modal basis functions to span the solution space in the homogeneous and regular waveguide regions (Ω_i). Consequently, we construct the finite dimensional subspace Λ^h as

$$\Lambda^h = \left(\boldsymbol{\mathcal{E}} \mid \boldsymbol{\mathcal{E}} = \begin{cases} \bar{\mathcal{E}}^I \underline{\boldsymbol{\alpha}}^I + \displaystyle\sum_{i=1}^{M} \bar{\mathcal{E}}^{\Gamma_i} \underline{\boldsymbol{\alpha}}^{\Gamma_i} & \text{in } \Omega_0 \\ \boldsymbol{\mathcal{E}}^i_{\text{inc}} + \displaystyle\sum_{n=1}^{N} a^i_n \boldsymbol{\mathcal{E}}^i_n & \text{in } \Omega_i \end{cases} \right), \tag{4}$$

where $\boldsymbol{\alpha}$ is the set of tangential vector basis functions, $\bar{}$ denotes a row vector, $\underline{}$ denotes a column vector, and M, N are the number of ports and the number of modes specified for each port, respectively. Notice that we have used two different types of basis functions in different regions. Furthermore, these two representations must be matched along the port reference plane in the sense described later.

Using the fact that modes of the waveguide are orthogonal, and from Eqs. (1) and (2), the boundary integrals in (3) can be integrated analytically to result in

$$\begin{aligned} \oint_{\Gamma_i} \boldsymbol{\mathcal{V}} \times \frac{1}{\mu_r} (\nabla \times \boldsymbol{\mathcal{E}}) \cdot d\mathbf{A} &= -j\mu_0\omega \oint_{\Gamma_i} \boldsymbol{\mathcal{V}} \times \mathbf{H} \cdot d\mathbf{A} \\ &= -jk_0 \sqrt{\frac{\mu_0}{\epsilon_0}} (\bar{c}^i [K^i] \underline{a}^i - \bar{c}^i [K^i] \underline{\delta}^i), \end{aligned} \tag{5}$$

where the unknowns a^i_j and c^i_j are the coefficients of the modes in $\boldsymbol{\mathcal{E}}$ and $\boldsymbol{\mathcal{V}}$, respectively, $[K^i]$ is the diagonal matrix defined by (2), and the column vector $\underline{\delta}^i$ is constructed in the following way: we set $\delta^i_j = 1$ if mode j is the excitation for the region i, otherwise $\delta^i_j = 0$. Furthermore, in the derivation of (5) a constant term has been dropped. In addition, we require the tangential continuity of both vector functions $\boldsymbol{\mathcal{E}}$ and $\boldsymbol{\mathcal{V}}$ along the port boundary Γ_i. This condition can be expressed for $\boldsymbol{\mathcal{E}}$ as

$$\underline{\mathcal{E}}^{\Gamma_i} = \underline{P}^i_{\text{inc}} + [P^i] \underline{a}^i, \quad \text{where } [P^i] = \left[\underline{P}^i_1, \ldots, \underline{P}^i_N \right]; \tag{6}$$

here $\underline{\mathcal{E}}^{\Gamma_i}$ is the projection of $\boldsymbol{\mathcal{E}}$ along the boundary edges on port Γ_i and $\underline{P}^i_j$ is the column of projections of mode $\boldsymbol{\mathcal{E}}^i_j$ along the boundary edges Γ_i.

2.3. *The Matrix Equation*

Finally, based on the above discussion, the bilinear from $B(\boldsymbol{\mathcal{E}}, \boldsymbol{\mathcal{V}})$ can be expressed in the matrix form as

$$B(\boldsymbol{\mathcal{E}}, \boldsymbol{\mathcal{V}}) = \bar{\mathcal{V}}[M]\underline{\mathcal{E}} + \sum_{i=1}^{M} jk_0\sqrt{\frac{\mu_0}{\epsilon_0}}\bar{c}^i[K^i]\underline{a}^i - \sum_{i=1}^{M} jk_0\sqrt{\frac{\mu_0}{\epsilon_0}}\bar{c}^i[K^i]\underline{\delta}^i, \tag{7}$$

where, taking into account Eq. (6), coefficient vectors are given by

$$\begin{aligned}\bar{\mathcal{V}} &= \left[\bar{\mathcal{V}}^I, \bar{P}^1_{\text{inc}} + \bar{c}^1[P^1]^T, \ldots, \bar{P}^M_{\text{inc}} + \bar{c}^M[P^M]^T\right]\\ \underline{\mathcal{E}} &= \left[\bar{\mathcal{E}}^I, \bar{P}^1_{\text{inc}} + \bar{a}^1[P^1]^T, \ldots, \bar{P}^M_{\text{inc}} + \bar{a}^M[P^M]^T\right]^T\end{aligned} \tag{8}$$

and matrix M is of the form

$$\begin{aligned}M_{ij} &= \int_{\Omega_0} (\nabla \times \boldsymbol{\alpha}_i) \cdot \frac{1}{\mu_r}(\nabla \times \boldsymbol{\alpha}_j) - k_0^2 \boldsymbol{\alpha}_i \cdot \epsilon_r \boldsymbol{\alpha}_j \, d\Omega,\\ [M] &= \begin{bmatrix} [M_{II}] & \left[M_{I\Gamma_1}\right] & \cdots & \left[M_{I\Gamma_M}\right] \\ \left[M_{\Gamma_1 I}\right] & \left[M_{\Gamma_1\Gamma_1}\right] & \cdots & \left[M_{\Gamma_1\Gamma_M}\right] \\ \vdots & \vdots & \ddots & \vdots \\ \left[M_{\Gamma_M I}\right] & \left[M_{\Gamma_M\Gamma_1}\right] & \cdots & \left[M_{\Gamma_M\Gamma_M}\right] \end{bmatrix}.\end{aligned} \tag{9}$$

For $\boldsymbol{\mathcal{E}}$ to be a solution of Eq. (1) in the Galerkin sense, the bilinear form $B(\boldsymbol{\mathcal{E}}, \boldsymbol{\mathcal{V}})$ must be equal to zero for all $\boldsymbol{\mathcal{V}}$ in Λ^h. This can be true only if the matrix equation

$$[\tilde{M}]\underline{\tilde{\mathcal{E}}} = \underline{\mathcal{Y}} \tag{10}$$

is satisfied, where

$$[\tilde{M}] = \begin{bmatrix} [M_{II}] & \left[M_{I\Gamma_1}\right][P^1] & \cdots & \left[M_{I\Gamma_M}\right][P^M] \\ [P^1]^T\left[M_{\Gamma_1 I}\right] & [P^1]^T\left[M_{\Gamma_1\Gamma_1}\right][P^1] + [\tilde{K}^1] & \cdots & [P^1]^T\left[M_{\Gamma_1\Gamma_M}\right][P^M] \\ \vdots & \vdots & \ddots & \vdots \\ [P^M]^T\left[M_{\Gamma_M I}\right] & [P^M]^T\left[M_{\Gamma_M\Gamma_1}\right][P^1] & \cdots & [P^M]^T\left[M_{\Gamma_M\Gamma_M}\right][P^M] + [\tilde{K}^M] \end{bmatrix} \tag{11}$$

and

$$\underline{\tilde{\mathcal{E}}} = [\bar{\mathcal{E}}^I, \bar{a}^1, \ldots, \bar{a}^M]^T, \quad [\tilde{K}^i] = jk_0\sqrt{\frac{\mu_0}{\epsilon_0}}[K^i], \tag{12}$$

$$\underline{\mathcal{Y}} = -\begin{bmatrix} \left[M_{I\Gamma_1}\right]P^1_{\text{inc}} + \left[M_{I\Gamma_2}\right]P^2_{\text{inc}} + \cdots + \left[M_{I\Gamma_M}\right]P^M_{\text{inc}} \\ [P^1]^T\left[M_{\Gamma_1\Gamma_1}\right]P^1_{\text{inc}} + \cdots + [P^1]^T\left[M_{\Gamma_1\Gamma_M}\right]P^M_{\text{inc}} - [\tilde{K}^1]\underline{\delta}^1 \\ [P^M]^T\left[M_{\Gamma_M\Gamma_1}\right]P^1_{\text{inc}} + \cdots + [P^M]^T\left[M_{\Gamma_M\Gamma_M}\right]P^M_{\text{inc}} - [\tilde{K}^M]\underline{\delta}^M \end{bmatrix}. \tag{13}$$

Notice that since the submatrices $[M_{ij}]$ are sparse and the number of modes N in the formulation is usually small enough, matrix multiplications can be done very efficiently. The final matrix is sparse and symmetric and can be solved by using the preconditioned conjugate gradient method (PCCG) or by the multilevel method described in the next section.

3. MULTI-*p* METHOD FOR THE *P*-VERSION OF THE FINITE ELEMENT ANALYSIS

Multigrid methods have been regarded as one of the most promising iterative methods for solving systems of linear equations arising from the discretization of partial differential equations by either the FDM or the h-version of the FEM [6, 14, 15]. For example, it has been shown in [16] that for the Poisson equation in a rectangular domain the convergence factor of a multigrid V-cycle method is bounded away from one independent of the mesh size h.

However, in general, there are two kinds of finite element methods: the h-version and the p-version. In the h-version polynomial basis functions are fixed over each element and accuracy is achieved by refining the mesh. In contrast, in the p-version the mesh is fixed and accuracy is achieved by increasing the degree p of polynomial basis functions.

Motivated by the success of multigrid methods for the h-version of the FEM, some researchers have applied multigrid ideas to equations arising from the p-version of the finite element analysis [17, 18]. The name *multi-p methods* has been proposed by Babushka [17], who also has conducted some numerical tests. It has been shown that the multi-p V-cycle methods converge faster than the classical Gauss–Seidel or SOR methods, but not as fast as the h-version multigrid methods.

Our objective in the following sections is to investigate the multi-p methods for the p-version of the transfinite element analysis. We will briefly discuss some of the properties of the p-version of the TFEM. Furthermore, we will present the multi-p V-cycle algorithm and show its convergence on representative sample problems.

3.1. *Hierarchical Transfinite Element Method*

The algorithm discussed in this section is based on the use of hierarchical bases of the type that is often used in the p-version of the adaptive mesh refinement. For example, if one has solved a problem for a given value of p, corresponding to a finite element space $\mathcal{M}_h$, one can enrich the space to say, order $p+1$ by adding certain hierarchical basis functions to the set of basis functions already used in $\mathcal{M}_h$. If $\bar{\mathcal{M}}_h$ is the new space, then we have the hierarchical decomposition

$$\bar{\mathcal{M}}_h = \mathcal{M}_h \oplus \mathcal{W}_h, \tag{14}$$

where $\mathcal{W}_h$ is the function space spanned by the new basis functions. But before we discuss the hierarchical transfinite element method, we should first describe the function space $\mathcal{H}^n(\text{curl};\Omega)$ which is defined by

$$\mathcal{H}^n(\text{curl};\Omega) = (\mathcal{P}^n(\Omega))^3 \oplus \mathcal{S}^{n+1}(\Omega) \tag{15}$$

and

$$\mathcal{S}^n(\Omega) = \{\boldsymbol{v} \mid \boldsymbol{v} \in (\bar{\mathcal{P}}^n(\Omega))^3, \boldsymbol{v}\cdot\boldsymbol{r} = 0\}. \tag{16}$$

In Eqs. (15) and (16), $\oplus$ means the direct sum, $\mathcal{P}^n(\Omega)$ is the set of piecewise polynomials which are complete to nth order, and $\bar{\mathcal{P}}^n(\Omega)$ is the set of polynomials which are exactly nth order in Ω, respectively. In other words, in this vector function space $\mathcal{H}^n(\text{curl};\Omega)$, the vector function $\boldsymbol{v}$ and its curl $\nabla\times\boldsymbol{v}$ will be at least complete to nth order for each of the vector components.

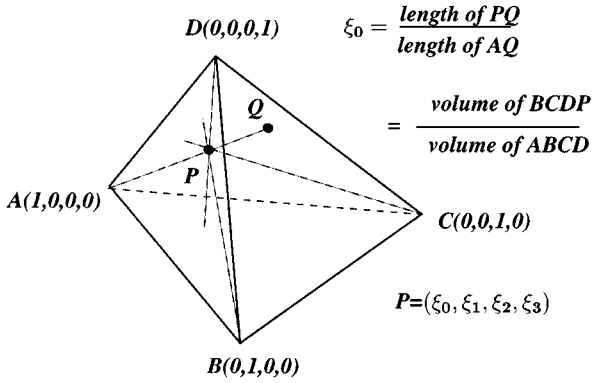

FIG. 2. Barycentric coordinates for a tetrahedron. Q is a point on face BCD.

We recall now that the basic idea of the transfinite element approach is to combine tangential vector finite element basis functions with modal basis functions to provide solutions for open boundary problems. Consequently, in the p-version of the transfinite element method we utilize both hierarchical vector finite element basis functions and modal basis functions.

We start our discussion with the description of hierarchical tangential vector finite element method (TVFEM) basis functions. Shown in Fig. 2 is a standard tetrahedral element. Each point of the tetrahedron is characterized by four barycentric coordinates, $\xi_0, \xi_1, \xi_2, \xi_3$, whose sum is always $\xi_0 + \xi_1 + \xi_2 + \xi_3 = 1$. In barycentric coordinate system the vertices of the tetrahedron become (1,0,0,0), (0,1,0,0), (0,0,1,0), and (0,0,0,1).

In general, the hierarchical vector basis functions for $\mathcal{H}^0(\text{curl}; \Omega)$ and $\mathcal{H}^1(\text{curl}; \Omega)$ can be divided into two groups: the edge vector basis functions and the face basis functions. Furthermore, the edge vector basis functions consist of edge-element basis functions and gradient type basis functions.

Edge vector basis functions.

$$\begin{aligned}
\boldsymbol{W}_0 &= \xi_0\nabla\xi_1 - \xi_1\nabla\xi_0, & \boldsymbol{W}_6 &= 4(\xi_0\nabla\xi_1 + \xi_1\nabla\xi_0),\\
\boldsymbol{W}_1 &= \xi_0\nabla\xi_2 - \xi_2\nabla\xi_0, & \boldsymbol{W}_7 &= 4(\xi_0\nabla\xi_2 + \xi_2\nabla\xi_0),\\
\boldsymbol{W}_2 &= \xi_0\nabla\xi_3 - \xi_3\nabla\xi_0, & \boldsymbol{W}_8 &= 4(\xi_0\nabla\xi_3 + \xi_3\nabla\xi_0),\\
\boldsymbol{W}_3 &= \xi_1\nabla\xi_2 - \xi_2\nabla\xi_1, & \boldsymbol{W}_9 &= 4(\xi_1\nabla\xi_2 + \xi_2\nabla\xi_1),\\
\boldsymbol{W}_4 &= \xi_1\nabla\xi_3 - \xi_3\nabla\xi_1, & \boldsymbol{W}_{10} &= 4(\xi_1\nabla\xi_3 + \xi_3\nabla\xi_1),\\
\boldsymbol{W}_5 &= \xi_2\nabla\xi_3 - \xi_3\nabla\xi_2, & \boldsymbol{W}_{11} &= 4(\xi_2\nabla\xi_3 + \xi_3\nabla\xi_2),
\end{aligned} \tag{17}$$

where the first six functions $\boldsymbol{W}_0, \ldots, \boldsymbol{W}_5$ are the edge-element vector basis functions, and the second six functions $\boldsymbol{W}_6, \ldots, \boldsymbol{W}_{11}$ are called gradient basis functions because they are products of the gradient operator applied to a scalar function.

Face vector basis functions. Furthermore, the eight basis functions associated with face unknowns are defined as

$$\begin{aligned}
\boldsymbol{W}_{12} &= 4\xi_2(\xi_1\nabla\xi_3 - \xi_3\nabla\xi_1), & \boldsymbol{W}_{13} &= 4\xi_3(\xi_1\nabla\xi_2 - \xi_2\nabla\xi_1),\\
\boldsymbol{W}_{14} &= 4\xi_2(\xi_0\nabla\xi_3 - \xi_3\nabla\xi_0), & \boldsymbol{W}_{15} &= 4\xi_3(\xi_0\nabla\xi_2 - \xi_2\nabla\xi_0),\\
\boldsymbol{W}_{16} &= 4\xi_1(\xi_0\nabla\xi_3 - \xi_3\nabla\xi_0), & \boldsymbol{W}_{17} &= 4\xi_3(\xi_0\nabla\xi_1 - \xi_1\nabla\xi_0),\\
\boldsymbol{W}_{18} &= 4\xi_1(\xi_0\nabla\xi_2 - \xi_2\nabla\xi_0), & \boldsymbol{W}_{19} &= 4\xi_2(\xi_0\nabla\xi_1 - \xi_1\nabla\xi_0),
\end{aligned} \tag{18}$$

and finally,

$$\begin{aligned}\mathcal{H}^0(\text{curl};\,\Omega) &= \text{span}\{\boldsymbol{W}_0, \boldsymbol{W}_1, \ldots, \boldsymbol{W}_5\}\\ \mathcal{H}^1(\text{curl};\,\Omega) &= \text{span}\{\boldsymbol{W}_0, \boldsymbol{W}_1, \ldots, \boldsymbol{W}_{19}\}.\end{aligned} \tag{19}$$

The above set of basis functions is hierarchic; that is, the finite element space $\mathcal{H}^0(\text{curl};\,\Omega)$ that is spanned by the basis functions with degree up to 1 is completely embedded into the space $\mathcal{H}^1(\text{curl};\,\Omega)$ that is spanned by the basis functions with degree up to 2.

Moreover, if we recall the modal basis functions representation from the previous section, that is, a modal basis function is a mode in a given waveguide region, then we can intuitively see that a combination of hierarchical vector basis functions and modal basis functions form a hierarchical set of basis functions for the p-version of transfinite element method. Consequently, the matrix $[\tilde{M}]$ and the right-hand side vector $\underline{\tilde{\mathcal{Y}}}$ in the matrix equation (10) also have hierarchical structures. For example, if we consider matrix equation $\tilde{M}^1\tilde{\mathcal{E}} = \tilde{\mathcal{Y}}^1$ corresponding to the $\mathcal{H}^1(\text{curl})$ TFEM it can be written in block form as

$$\begin{bmatrix}\tilde{M}_{11} & \tilde{M}_{12}\\ \tilde{M}_{21} & \tilde{M}_{22}\end{bmatrix}\begin{bmatrix}\tilde{\mathcal{E}}_1\\ \tilde{\mathcal{E}}_2\end{bmatrix} = \begin{bmatrix}\tilde{\mathcal{Y}}_1\\ \tilde{\mathcal{Y}}_2\end{bmatrix}, \tag{20}$$

where $\tilde{M}_{11}$ and $\tilde{\mathcal{Y}}_1$ correspond to the $\mathcal{H}^0(\text{curl})$ version of TFEM equation $\tilde{M}^0\tilde{\mathcal{E}} = \tilde{\mathcal{Y}}^0$; that is, $\tilde{M}^0 \approx \tilde{M}_{11}$ and $\tilde{\mathcal{Y}}^0 \approx \tilde{\mathcal{Y}}_1$.

3.2. *Two-level V-Cycle Algorithm*

The basic idea behind the p-version of a multilevel algorithm is to accelerate the solution process of a set of fine-level equations by computing the corrections on a coarser level. We start with eliminating the high frequency errors associated with an initial solution on the fine level, using iterative matrix solvers (the Gauss–Seidel iterative method and the conjugate gradient method) [1, 2]. Once this is achieved, we compute a residual vector and transfer it to a coarser level where the system of equations corresponding to the coarsest level must be solved directly [6] to compute a correction vector to our solution. The coarse-level correction is then interpolated back to the fine level in order to update the solution vector and eliminate low frequency errors. The entire process is then repeated until the desired accuracy for the solution is achieved. Furthermore, in the above process we need to define prolongation (interpolation) and projection (restriction) operators, as well as the matrix equation on the coarse level and the method of its solution.

The prolongation operator I_0^1 corresponding to the mapping form $\mathcal{H}^0(\text{curl})$ space to the $\mathcal{H}^1(\text{curl})$ space for the p-version of transfinite element approach is simply defined by the injection mapping. Furthermore, the projection operator I_1^0 is defined as $I_1^0 = (I_0^1)^T$. Based on the p-version and hierarchical basis functions, the defined prolongation and projection operators can be express in the matrix form as

$$I_0^1 = \begin{bmatrix}I_0\\ 0\end{bmatrix}, \quad I_1^0 = [I_0 \quad 0], \tag{21}$$

where I_0 is the $N_0 \times N_0$ identity matrix, and N_0 is the number of unknowns corresponding to the $\mathcal{H}^0(\text{curl})$ system of equations.

In comparison with the *h*-version multigrid methods, the prolongation and projection here are very simple and independent of the domain geometry. Moreover, it is easy to verify that the prolongation and projection operators satisfy the relation

$$\tilde{M}^0 \approx I_1^0 \tilde{M}^1 I_0^1. \tag{22}$$

Equation (22) is not an equality because the modal basis functions at the ports computed using $\mathcal{H}^0(\text{curl})$ FEM are different from the projection of the $\mathcal{H}^1(\text{curl})$ modal basis functions on the $\mathcal{H}^0(\text{curl})$ space.

Finally, to present a two-level multi-p V-cycle method in matrix form we consider matrix equation $\tilde{M}^1\tilde{\mathcal{E}} = \tilde{\mathcal{Y}}^1$ corresponding to the $\mathcal{H}^1(\text{curl})$ TFEM and rewrite it in block form as

$$\begin{bmatrix} \tilde{M}_{11} & \tilde{M}_{12} \\ \tilde{M}_{21} & \tilde{M}_{22} \end{bmatrix} \begin{bmatrix} \tilde{\mathcal{E}}_1 \\ \tilde{\mathcal{E}}_2 \end{bmatrix} = \begin{bmatrix} \tilde{\mathcal{Y}}_1 \\ \tilde{\mathcal{Y}}_2 \end{bmatrix}, \tag{23}$$

where $\tilde{M}^0 \approx \tilde{M}_{11}$. The multi-$p$ algorithm can then be given as follows.

ALGORITHM.

1. Solve the matrix equation $\tilde{M}^0\tilde{\mathcal{E}}_1 = \tilde{\mathcal{Y}}^0$ on the coarser level to find an initial guess $[\tilde{\mathcal{E}}_1, 0]$.
2. Perform μ iterations of the matrix equation $\tilde{M}^1\tilde{\mathcal{E}} = \tilde{\mathcal{Y}}^1$ using the Gauss–Seidel iterative solver, and let the solution be $\tilde{\mathcal{E}}^\mu = [\tilde{\mathcal{E}}_1^\mu, \tilde{\mathcal{E}}_2^\mu]$.
3. Solve matrix equation $\tilde{M}^0 e^0 = I_1^0(\tilde{\mathcal{Y}}^1 - \tilde{M}^1\tilde{\mathcal{E}}^\mu)$ using the direct solver to correct the solution vector on the finer level $\tilde{\mathcal{E}}^{\mu+1} = \tilde{\mathcal{E}}^\mu + I_0^1(e^0)$.
4. If the residual is within the tolerance, stop; otherwise, go back to step 2 with the initial vector $\tilde{\mathcal{E}}^{\mu+1}$.

In the following section we will analyze the performance of the two-level multi-p V-cycle algorithm for different examples and different values of parameter μ.

4. NUMERICAL EXAMPLES

In this section we present a number of sample problems that have been solved by using the two-level multi-p method described in the previous section. First, a simple waveguide problem will be discussed. Then we will apply the method to a mitered bend example and to a shielded microstrip problem. Finally, a rectangular waveguide with a dielectric obstacle will be considered. For each of the above examples we will analyze the convergence behavior of the multi-p V-cycle algorithm for different frequencies, as well as for different values of parameter μ which corresponds to the number of fine-level relaxations or sweeps between coarse-level corrections. Furthermore, for the waveguide problem two different discretizations will be used and the convergence behavior will be compared.

It will be shown that in order for the multi-p method to work, an additional relation between the operating frequency f and the mesh size h must be satisfied. Consequently, it will be demonstrated on different examples that the convergence rate of the multi-p V-cycle algorithm is a function of frequency and discretization, as well as parameter μ. Moreover, an adaptive multi-p V-cycle will be introduced to minimize the computation time. Finally, to prove the computational efficiency of the multi-p method, the number of iterations required to achieve a given accuracy by using the ICCG [2] will be compared with the number of iterations for the multi-p V-cycle solver for each example.

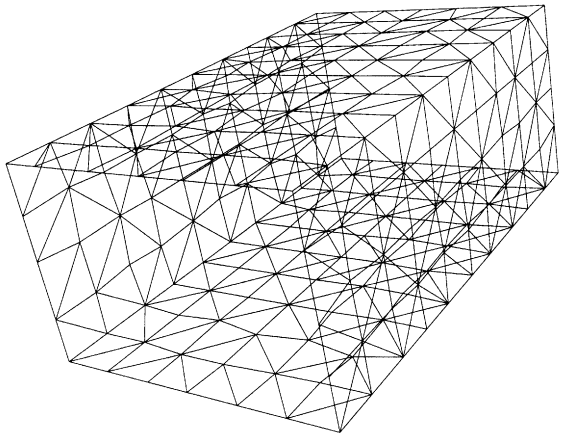

FIG. 3. The rectangular waveguide and discretization on the PEC boundary, coarse mesh.

4.1. *Rectangular Waveguide*

In the first example, the multi-p V-cycle algorithm is used to analyze a rectangular waveguide (width $= 3$ m, height $= 2$ m, length $= 5$ m), depicted in Fig. 3, filled with air. A coarse discretization corresponds to the mesh size $h \approx 0.7$ m and the operating frequency $f = 100$ MHz, and it is approximately six tetrahedral elements per wavelength. Only dominant modes have been used to interpolate the electric field within each waveguide region, and the excitation has been chosen to be the dominant mode of any of the two waveguide ports. The multi-p V-cycle has been applied for different values of parameter μ corresponding to the number of fine-level sweeps between coarse-level corrections.

Shown in Fig. 4 is the norm of the relative residual (residual divided by the norm of the right-hand side vector) as a function of the number of iterations (number of sweeps on the fine level) for different values $\mu = 1, 3, 5$. As it can be seen from this figure it does not matter what choice of μ we choose, the multi-p V always diverges. This effect can be explained

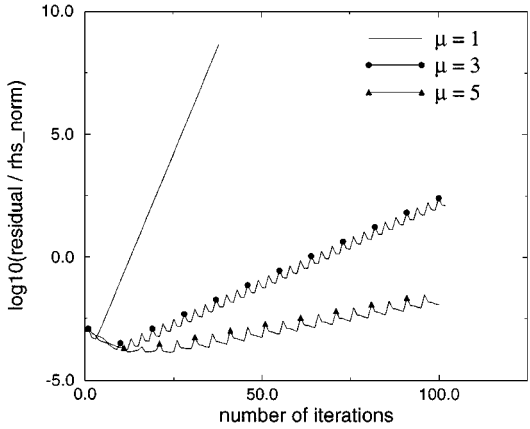

FIG. 4. The convergence behavior of the V-cycle for different values of parameter μ, $f = 100$ MHz, coarse discretization.

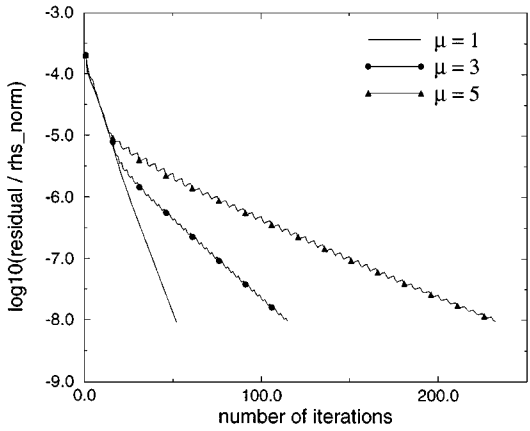

FIG. 5. The convergence behavior of the V-cycle for different values of parameter μ, $f = 55$ MHz.

if we come back and recall that the multi-p method works if and only if the low frequency errors are suitably reduced by the coarse-level corrections. Consequently, the coarser level should be fine enough to provide a rough approximation to the low frequency eigenvalues. Otherwise the low frequency errors will be magnified and the method will diverge. That is exactly the case in the given example.

One way to make sure that the low frequency eigenvalues are correctly approximated on the coarse level is to decrease the mesh size h. However, we may as well decrease the operating frequency, which is equivalent to the smaller mesh size. Shown in Fig. 5 is the convergence behavior of the multi-p V-cycle method for the same example with the same discretization as on Fig. 3 but for the operating frequency $f = 55$ MHz, which corresponds to approximately 11 tetrahedral elements per wavelength. One can observe a dramatic change in the behavior of the multi-p method—it converges now. Furthermore, if we denote one relaxation sweep (RS) on the fine level as one operation and assume that the coarse-grid correction (CGC) process (restriction + solution on coarse level + interpolation) is time equivalent to one operation on the fine level, then the total number of operations for $\mu = 1$ is equal to $52(\text{RS}) + 52(\text{CGC}) = 104$, for $\mu = 2$—$72(\text{RS}) + 36(\text{CGC}) = 108$, for $\mu = 3$—$115(\text{RS}) + 38(\text{CGC}) = 153$, and so on. As can be seen from Fig. 5, the number of operations is minimum for $\mu = 1$ value, or in other words, if the coarse-level correction is done right after each relaxation sweep on the fine level.

However, this number of iterations can be reduced even more if we adjust μ dynamically. That is, relaxation sweeps on the fine level should be discontinued and a switch should be made to a coarse-level correction when the rate of convergence becomes slow, namely

$$\frac{\text{residual norm}}{\text{residual norm a sweep earlier}} \geq \eta. \tag{24}$$

An appropriate value of η may easily be found by direct trials. Such a value is typical to the problem and is independent of frequency or mesh size. For the given example we have obtained the minimum number of operations to be 97 (52 RS and 45 CGC) for $\eta = 0.78$. To compare, it takes 120 iterations for ICCG to converge with the same accuracy, and each iteration is equivalent roughly to one fine-level sweep plus the solution of the preconditioner matrix equation on the fine level.

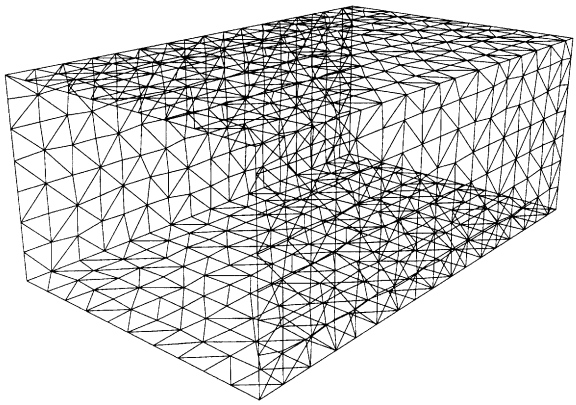

FIG. 6. The rectangular waveguide and discretization on the PEC boundary, fine mesh.

Furthermore, we have analyzed the same example but using a different discretization shown in Fig. 6 which corresponds to the mesh size $h \approx 0.42$ m. If we choose the operating frequency $f = 100$ MHz it results in approximately 11 tetrahedral elements per wavelength. Our objective now is to show that the multi-p V-cycle will work for this frequency, even though it failed for the coarser discretization.

Presented on Fig. 7 is the norm of the residual divided by the norm of the right-hand side versus the number of iterations for different values of parameter $\mu = 1, 3, 5$. The method converges for this mesh since the low frequency eigenvalues are now approximated correctly on the coarse level and the error in low frequencies is decreased after each coarse-level correction. The minimum number of operations to achieve the final relative residual 10^{-7} is equal to 71 (39 RS and 32 CGC), corresponding to the $\eta = 0.78$ value. One can compare it with 80 operations (40 RS, 40 CGC) for $\mu = 1$, 76 operations (52 RS, 26 CGC) for $\mu = 2$, or 297 iterations of ICCG.

Finally, if one tries to solve the rectangular waveguide problem for the fine discretization, but for the operating frequency $f = 200$ MHz, the multi-p algorithm once again fails

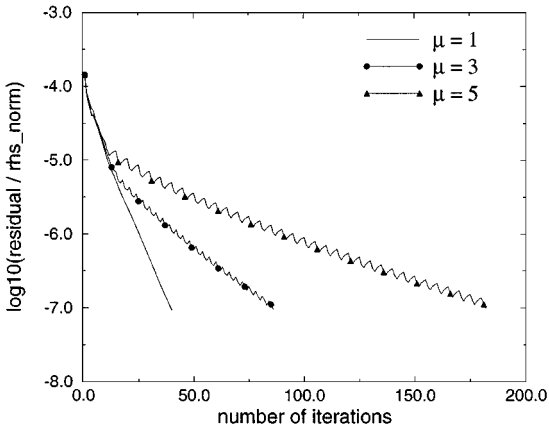

FIG. 7. The convergence behavior of the V-cycle for different values of parameter μ, $f = 100$ MHz, fine discretization.

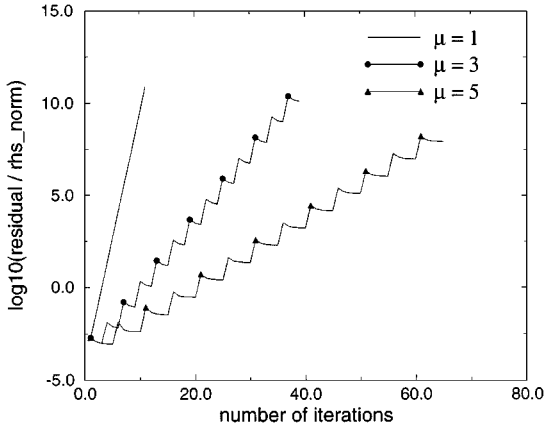

FIG. 8. The convergence behavior of the V-cycle for different values of parameter μ, $f = 200$ MHz, fine discretization.

(Fig. 8). It is expected, since this frequency corresponds to approximately six elements per wavelength, and the coarse-level correction does not reduce low frequency errors any more. Consequently, to ensure that the multi-p V-cycle algorithm converges using the Gauss–Seidel smoothing, an additional requirement must be satisfied. That is, the coarse-grid level should be fine enough to provide a rough approximation to the low frequency eigenfunctions, especially to eigenfunctions corresponding to the negative eigenvalues of the matrix equation.

4.2. *Mitered Bend*

As the second sample example, a mitered bend has been considered. Shown in Fig. 9 is the mitered bend filled with air. Furthermore, the reflection coefficient versus frequency

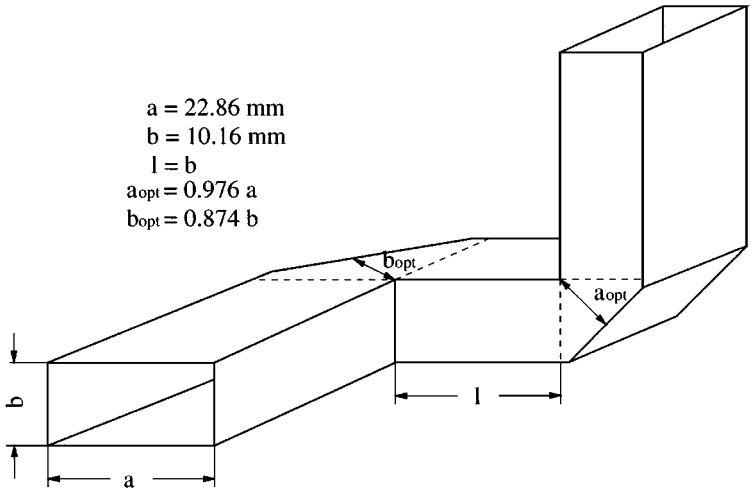

FIG. 9. Mitered 90 H-plane and E-plane bends.

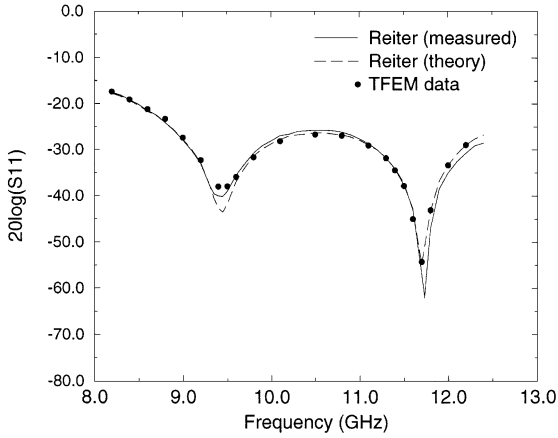

FIG. 10. Reflection coefficient as a function of frequency for the mitered bend.

for this example is plotted in Fig. 10 and compared with previously published results from [19]. First the problem domain has been discretized with mesh size $h \approx 3$ mm, which corresponds to 14,670 tetrahedral elements or 86,604 unknowns for the $\mathcal{H}^1(\text{curl})$ TFEM. Only dominant modes have been used to describe the electric field within the waveguide regions, and the excitation has been chosen to be the dominant mode of one of the ports. This example has been analyzed for different frequencies to compare the performance of the multi-p V-cycle algorithm with the ICCG solver.

We start the analysis by taking the operating frequency to be $f = 8$ GHz. The convergence behavior of the V-cycle algorithm for different values of parameter μ is depicted in Fig. 11. For example, it takes 86 operations (43 RS, 43 CGC) for $\mu = 1$, 65 operations (43 RS, 22 CGC) for $\mu = 2$, or 73 operations (55 RS, 18 CGC) for $\mu = 3$ to achieve the same accuracy. Furthermore, the minimum number of iterations equals 65 operations (46 RS and 19 CGC) for $\eta = 0.83$, which is exactly the same as the number of operations for $\mu = 2$. As one will see later, in most cases if one chooses $\mu = 2$ the total number of operations will be

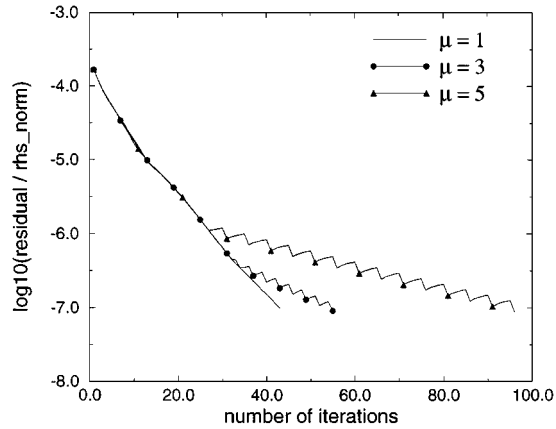

FIG. 11. The convergence rate of the V-cycle algorithm for different values of μ, $f = 8$ GHz, bend example.

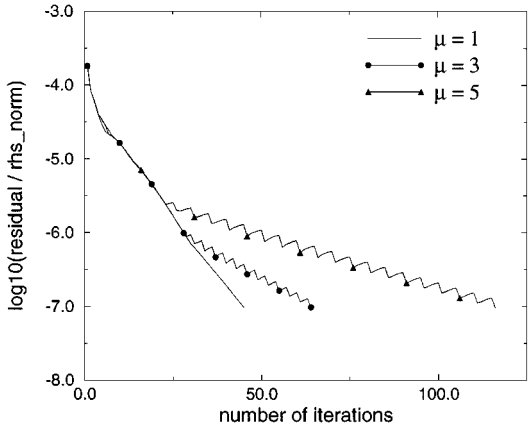

FIG. 12. The convergence rate of the V-cycle algorithm for different values of μ, $f = 10$ GHz, bend example.

close to the minimum. To compare, it takes 590 iterations for ICCG to converge with the same accuracy.

We have also analyzed the above example for frequencies $f = 10$ GHz and $f =$ 12 GHz. For both frequencies the relative residual versus the number of iterations has been plotted (Fig. 12 and Fig. 13) for different values of μ. For example, for the operating frequency $f = 10$ GHz it takes 95 operations (45 RS, 45 CGC) for $\mu = 1$, 68 operations (45 RS, 23 CGC) for $\mu = 2$, and 85 operations (64 RS, 21 CGC) for $\mu = 3$ to converge to the final relative residual 10^{-7}. The minimum number of operations for the adaptive V-cycle is equal to 69 (47 RS, 22 CGC) for $\eta = 0.82$. It takes 608 iterations for ICCG to achieve the same accuracy.

Finally, by choosing the operating frequency to be $f = 12$ GHz one can get the following results. It takes 96 operations (48 RS, 48 CGR) for $\mu = 1$, 74 operations (49 RS, 25 CGC) for $\mu = 2$, and 102 operations (76 RS, 26 CGC) for $\mu = 3$ to converge with the final relative residual 10^{-7}. The minimum number of operations for the adaptive V-cycle equals 75 (50 RS, 25 CGC). The ICCG converges to the same error in 690 iterations.

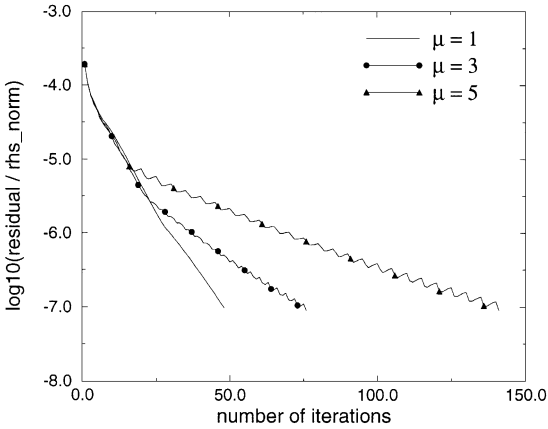

FIG. 13. The convergence rate of the V-cycle algorithm for different values of μ, $f = 12$ GHz, bend example.

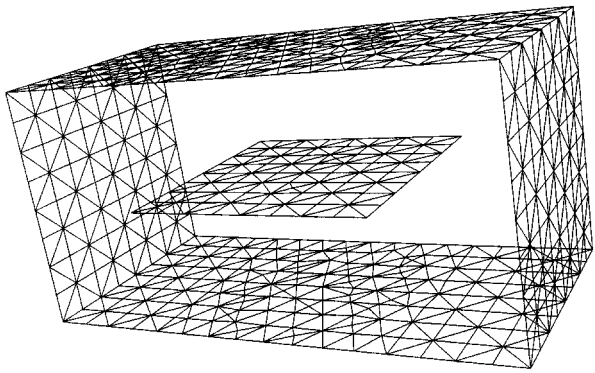

FIG. 14. Geometry and surface discretization of the shielded microstrip line, filled with air and dielectric $\epsilon_r = 5$. Width = 2 m, height = 1 m, length = 1 m, strip width = 1 m.

4.3. *Shielded Microstrip Line*

Shown in Fig. 14 is a shielded microstrip line that has been chosen as the third example. Also shown is the surface discretization of the problem domain, corresponding to the mesh size $h \approx 0.18$ m, which results in 12,222 tetrahedral elements or consequently in 73,534 unknowns for the $\mathcal{H}^1(\text{curl})$ TFEM. This example has been analyzed for different frequencies: $f = 300$ MHz, $f = 700$ MHz, and $f = 1000$ MHz. The dependence of the relative residual versus the number of iterations is presented in Figs. 15–17. Furthermore, given in Table 1 is the comparison of the multi-p V-cycle method for different values of parameter μ with the ICCG method. For each value of μ the total number of operations is shown which equals the number of relaxations sweeps plus the number of coarse grid corrections (RS + CGC). It is worth mentioning that the results for the adaptive V-cycle have been obtained by taking $\eta = 0.73$. Finally, given in Table 2 is the number of operations for the adaptive V-cycle for different η. As one can see the number of operations is extremely sensitive to the η value.

4.4. *Dielectric Obstacle in Rectangular Waveguide*

In the last example we have investigated a rectangular waveguide with a dielectric obstacle inside (shown in Fig. 18). The parameter a and the operating frequency f have been chosen to be 1 m and 95 MHz, respectively. Furthermore, the relative permittivity ϵ_r for the dielectric obstacle equals 6. Depicted in Fig. 19 is the reflection coefficient versus the frequency, compared with the results from [20].

TABLE 1

Frequency (MHz)	Number of operations N (RS, CGC)				Number of ICCG iterations
	$\mu = 1$	$\mu = 2$	$\mu = 3$	Adaptive	
$f = 300$	60 (30, 30)	48 (32, 16)	52 (39, 13)	48 (34, 14)	222
$f = 700$	70 (35, 35)	61 (40, 21)	75 (56, 19)	62 (32, 30)	234
$f = 1000$	82 (41, 41)	70 (46, 24)	86 (64, 22)	71 (49, 22)	341

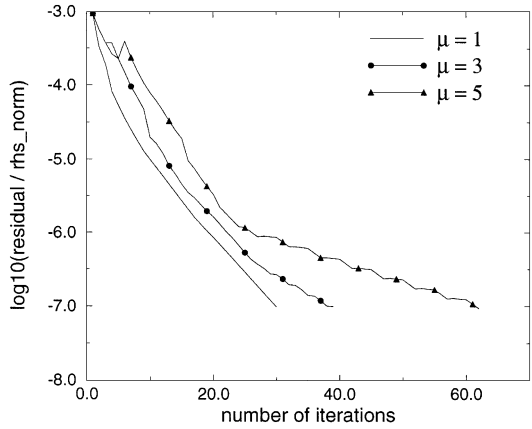

FIG. 15. The convergence rate for the microstrip example corresponding to $f = 300$ MHz for different values of μ.

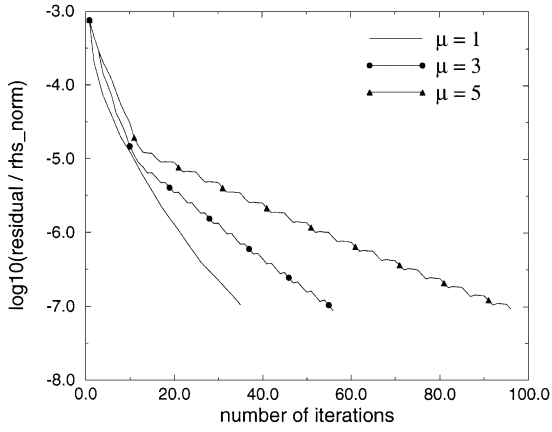

FIG. 16. The convergence rate for the microstrip example corresponding to $f = 700$ MHz for different values of μ.

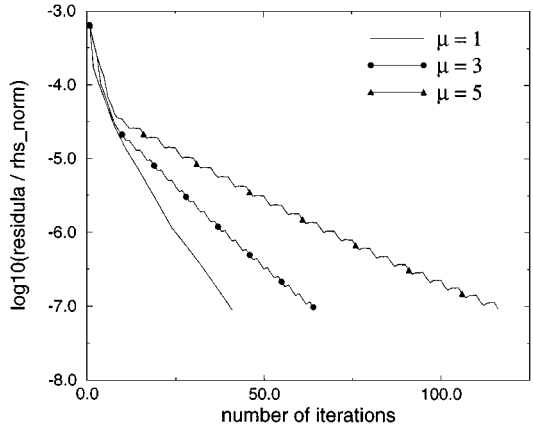

FIG. 17. The convergence rate for the microstrip example corresponding to $f = 1000$ MHz for different values of μ.

TABLE 2

η	0.67	0.71	0.72	0.73	0.74	0.75	0.76	0.77	0.78	0.79	0.8	0.85
# RS	41	41	43	49	57	58	59	62	65	66	67	70
# CGC	38	38	35	22	22	22	22	22	22	22	22	22
Total	79	79	78	71	79	80	81	84	87	88	89	92

First the computational domain has been discretized with mesh size $h \approx 0.15$ m within the dielectric obstacle and $h \approx 0.3$ m in the air region. This resulted in 12,260 tetrahedral elements and 74,692 unknowns for the $\mathcal{H}^1(\text{curl})$ TFEM. We have studied the convergence behavior of the multi-p V-cycle method for two different cases: (i) when only the dominant mode is taken to interpolate fields in the waveguide regions, and (ii) when the first three modes are taken. For each case we have plotted the convergence rate for different values of parameter μ.

Plotted in Fig. 20 is the convergence of the V-cycle when only one mode is assigned for each port. It takes 116 operations (58 RS, 58 CGC) for $\mu = 1$, 86 operations (57 RS, 29 CGC) for $\mu = 2$, and 107 operations (80 RS, 27 CGC) for $\mu = 3$ to converge to the final residual 10^{-8}. The minimum number of operations for the adaptive V-cycle is achieved when $\eta = 0.79$ and it equals 86 operations (60 RS, 26 CGC). In comparison it took ICCG 276 iterations to achieve the same accuracy.

Finally, shown in Fig. 21 is the convergence rate of the V-cycle algorithm when the first three modes are assigned for each port. All computations have been conducted by using the V-cycle algorithm, but, since the convergence behavior for this case case is exactly the same as for the previous one, no separate data are presented. However, it took ICCG 313 iterations to converge to the same error.

5. CONCLUDING REMARKS

In this paper we discussed multigrid methods that had been developed for accelerating the convergence of iterative methods by using a sequence of grids ("levels") of increasing

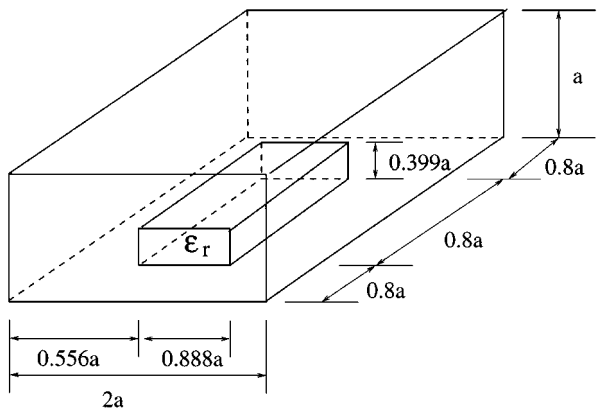

FIG. 18. Geometry of the rectangular waveguide with dielectric obstacle.

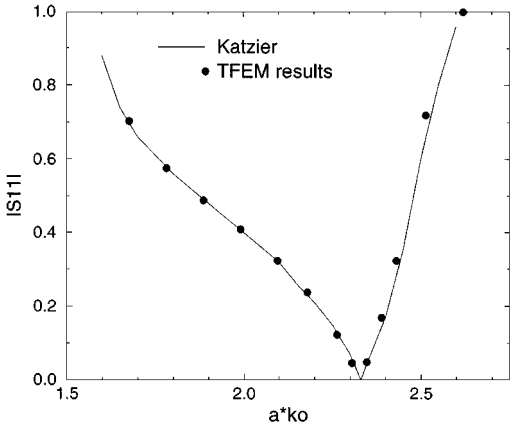

FIG. 19. Reflection coefficient vs frequency, dielectric obstacle. Reference results obtained by using the method of orthogonal expansions.

fineness, each of which may be introduced and changed in the process and constantly interacts with each other, and each grid ("level") is responsible for eliminating a particular frequency bandwidth of errors. The convergence behavior of these methods is considered to be optimal.

In this work we made an attempt to combine the multigrid concept with the p-version of the transfinite element approach that had been implemented for the analysis of unbounded problems such as MMIC devices and 3D waveguide junctions. To achieve this goal we have developed a two-level V-cycle algorithm and studied its performance on sample problems. Furthermore, in order to minimize the number of operations required for the multi-p method to converge to a given error, an adaptive V-cycle algorithm has been implemented and compared with the standard V-cycle for each example. Based on the numerical results and the description of the multi-p V-cycle algorithm that has been shown in previous sections,

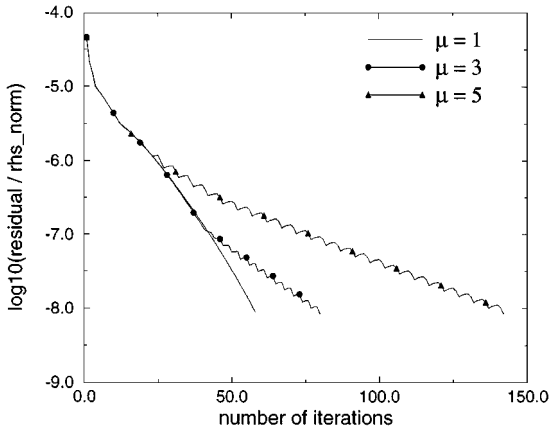

FIG. 20. The convergence behavior of the V-cycle for the rectangular waveguide with dielectric obstacle, $f = 95$ MHz. One mode is assigned for each port.

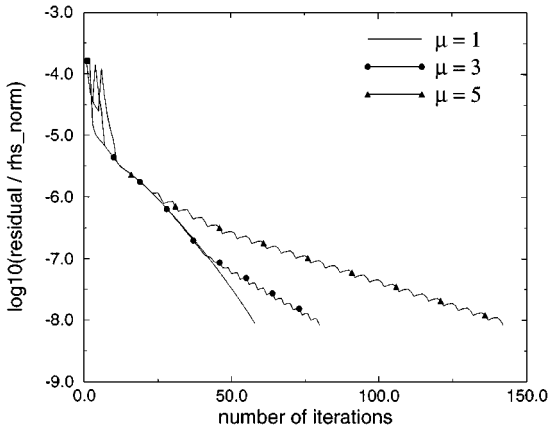

FIG. 21. The convergence behavior of the V-cycle for the rectangular waveguide with dielectric obstacle, $f = 95$ MHz. Three modes are assigned for each port.

we can make some conclusions as well as discuss the advantages and disadvantages of this approach.

First, it seems like the multi-p V-cycle algorithm is competitive with the ICCG method in terms of efficiency; that is, it requires much less computational effort. Furthermore, it turns out that the best performance of the V-cycle algorithm is achieved when the coarse-level correction is performed after each two relaxation sweeps on the fine level. The number of operations in this case is close to the minimum number of operations achieved by the adaptive V-cycle algorithm. This is important since for the adaptive method the η value for which the minimum number of operations is achieved cannot be predicted in advance, it can only be found by trials, and this value is different for different problem geometries.

Second, the convergence rate of the multi-p method is a function of frequency as well as mesh size; that is, if the frequency increases the convergence rate of the method becomes worse. This is due to the fact that the low-frequency eigenfunctions are not approximated accurately enough on the coarsest level. As has been shown, if the coarsest level is not fine enough the method diverges. Consequently, additional care must be taken concerning the coarsest level; it should be fine enough to provide a good approximation to low frequency eigenfunctions, especially to eigenfunctions corresponding to the negative eigenvalues of the matrix equations.

Finally, since on the coarsest level an indefinite problem should be solved directly, one needs to factorize the coarse-level matrix in order to perform coarse-grid corrections efficiently. Subsequently, if the number of unknowns on the coarsest level is large the factorization process can be very time consuming. Further research should be conducted in order to avoid the factorization and to solve a system of linear equations corresponding to the coarsest level more efficiently. An algebraic multigrid method might be viewed as a possible solution of this problem.

REFERENCES

1. R. S. Varga, *Matrix Iterative Analysis* (Prentice–Hall, Englewood Cliffs, NJ, 1962).
2. G. H. Golub and C. F. Van Loan, *Matrix Computations* (Johns Hopkins Univ. Press, Baltimore, MD, 1991).

3. W. L. Briggs, *A Multigrid Tutorial* (Soc. Indus. Appl. Math., Philadelphia, 1987).
4. W. Hackbusch and U. Trottenberg, *Multigrid Methods* (Springer-Verlag, Berlin, 1982).
5. S. McCormick, *Multigrid Methods* (SIAM, Philadelphia, 1987). [SIAM Frontiers Series, Vol. 3]
6. A. Brandt, Multi-level adaptive solutions to boundary-value problems, *Math. Comp*. **31**(138), 333 (1977).
7. A. Settari and K. Aziz, A generalization of the additive correction methods for the iterative solution of the matrix equations, *SIAM J. Numer. Anal*. **10**(3), 506 (1973).
8. R. A. Nicolaides, On some theoretical and practical aspects of multigrid methods, *Math. Comp*. **33**(147), 933 (1979).
9. R. A. Nicolaides, On multiple grid and related techniques for solving discrete elliptic systems, *J. Comput. Phys*. **19**, 418 (1975).
10. R. A. Nicolaides, On multigrid convergence in the indefinite case, *Math. Comp*. **32**(144), 1082 (1978).
11. Z. J. Cendes and J.-F. Lee, The transfinite element method for modeling MMIC devices, *IEEE Trans. Microwave Theory Tech*. **36**(12), 1639 (1988).
12. J.-F. Lee, *Finite Element Methods for Modeling Passive Microwave Devices*, Ph.D. thesis, Carnegie Mellon University, 1989.
13. S. V. Polstyanko and J.-F. Lee, $H_1(\mathrm{curl})$ tangential vector finite element method for modeling anisotropic optical fibers, *J. Lightwave Technol*. **13**(11), 2290 (1995).
14. R. A. Nicolaides, On the l^2 convergence of an algorithm for solving finite element equations, *Math. Comp*. **31**(140), 892 (1977).
15. R. E. Bank and T. Dupont, An optimal order process for solving finite element equations, *Math. Comp*. **36**(153), 35 (1981).
16. D. Braess and W. Hackbusch, A new convergence proof for the multigrid method including the V-cycle, *SIAM J. Numer. Anal*. **20**(5), 967 (1983).
17. I. Babuška and M. Suri, The optimal convergence rate of the p-version of the finite element method, *SIAM J. Numer. Anal*. **24**(4), 750 (1987).
18. N. Hu and I. N. Katz, Multi-P methods: Iterative algorithms for the P-version of the finite element analysis, *SIAM J. Sci. Comput*. **16**(6), 1308 (1995).
19. J. M. Reiter and F. Arndt, Rigorous analysis of arbitrarily shaped h- and e-plane discontinuities in rectangular waveguides by a full-wave boundary contour mode-matching method, *IEEE Trans. Microwave Theory Tech*. **43**(4), 796 (1995).
20. H. Katzier, Streuverhalten Elektromagnetischer Wellen bei Sprunghaften Übergängen Geschirmter Dielektrischer Leitungen, *Arch. Elek. Übertragung*. **38**, 290 (1984).